

**Borehole Video Survey and Assessment for Geophysical Anomaly  
Confirmation**  
**Dry Comal Creek Flood Retarding Structure**  
**Comal County, Texas**

Prepared for:

**Freese and Nichols, Inc.**

10814 Jollyville Rd.

Building 4, Suite 100

Austin, TX 78759

Prepared by:

Blake Weissling, PhD

**SWCA Environmental Consultants**

**6200 UTSA Blvd., Suite 102**

San Antonio, Texas 78249

**31 Aug 2010**

## **1.0 OBJECTIVE**

SWCA Environmental Consultants (SWCA) was contracted by Freese and Nichols, Inc. (FNI) to collect and interpret borehole video at the construction site of the Dry Comal Creek Flood Retarding Structure, Comal County, Texas for the purpose of evaluating and confirming near-surface karst-related geophysical anomalies. Twenty-eight percussion boreholes at depths ranging from 30 to 82 feet were drilled the week of 26 – 30 April, 2010 at various locations within the footprint and flanks of the excavation. Full color, digital video was obtained from 26 boreholes using a Laval R-Cam 1000 borehole video system. The primary goal of this phase of the site investigation was to document subsurface karst development in the context of the electrical resistivity and ground penetrating radar geophysical results from Phase I of this project (SWCA, 2010). SWCA geologist Guy Rubio with the assistance of SWCA geophysicist, Dr. Blake Weissling, conducted the field work and video acquisition. Dr. Weissling evaluated and interpreted the video records in the context of the geophysical results.

## **2.0 INSTRUMENTATION**

The instrumentation utilized for the borehole video survey for the Dry Comal Flood Retaining Structure (DCFRS) was a Laval Underground Surveys, Inc. (<http://www.lavalunderground.com>) Laval R-Cam 1000 borehole video system. The R-Cam collects and records full-color digital video in both down and side-looking views. Both video cameras are in full remote control by the surface operator who is also in full control of the descent and retreat rates of the video logging tool. The video stream is recorded on DVD at the surface console.

## **3.0 RESULTS AND DISCUSSION**

### **3.1 Stilling basin borehole evaluation**

Eight percussion boreholes (PB-5, PB-6, PB-7, PB-8, PB-9, PB-10, PB-25, and PB-28) were completed around the perimeter of the stilling basin excavation and were sited primarily to evaluate and/or confirm specific ground penetrating radar (GPR) anomalies detected and delineated in Phase 1 of this project. Borehole PB-5 was the first to be drilled and thus served as the primary site for perfecting the operation of the camera system. Video was recorded both in descending and ascending mode, as it would be for all subsequent boreholes. PB-5 was situated approximately 16 ft (5 m) from the west end of GPR line 50, and was positioned to evaluate a broad band of strong radar reflections at a depth of 5 – 16 ft (1.5 – 5 m) and extending the majority of the length of the radar profile. Examination of the borehole video revealed a zone of

karstic limestone, composed of a mix of apparent collapse breccia, solution-altered rock (honeycomb), and clay (terra rosa) with a high percentage of air-filled void space. This void space is predominately seen to occur in gaps between breccia and collapse material, but is also seen in association with clay in the honeycomb structure. Honeycomb or breccia zones with at least 25% air space, by visual estimation, were subsequently annotated as being most likely to exhibit high electrical resistivity as well as potentially reflective of near surface radar energy. Along with any large air-filled voids or caves encountered, the locations of highly porous zones (as described above) were subsequently converted to pictorial log format to emulate the driller's record. Orange zones in the logs represent highly porous, karst-altered rock most likely to generate resistive anomalies in the electrical resistivity imaging (ERI) geophysical profiles. Red zones depict actual caves or large voids (> 1 ft) encountered. Blue zones depict the water-filled portion of the borehole (when present), interpreted as the apparent water table.

Figure 1 shows GPR line 50 with the overlay of the PB-5 borehole video log, scaled to the depth scale of the radar profile. As it pertains to all subsequent discussion of the radar profiles, it should be noted here that the depth scale on all radar profiles is not absolute, but rather “the best guess” based on estimates of the radar velocity in the rock materials encountered at the site. The close match of the orange air-filled zones to the zone of high amplitude reflections in the profile does suggest that these porous karst zones are the origin of the observed radar anomalies. The match also suggests our estimate of the radar velocity was appropriate.

GPR line 38 in association with the PB-6 video log is shown in Figure 2. Once again, a close match was seen between the porous air-filled karst observed in the video and the zone of radar anomalies.

The target for the siting of PB-7 was the small amplitude anomaly seen at position 27 in GPR line 30. In actuality the location of the borehole was a meter or two east of line 30 (between 30 and 31). An overlay of the PB-7 video log on line 30 and line 31 can be seen in Figures 3 and 4, respectively. There is a small zone of air-filled karst at a depth of approximately 11 ft (3.5 m) that does not match with the shallower radar anomaly on line 30. As this anomaly is completely absent on line 31 (Figure 4), it is likely that this karst feature does not extend to the location of the borehole. Borehole PB-10 was located near the end of line 30 at position 50 (position 4 on line 31). There were no significant radar reflections observed from this corner of the stilling basin and likewise no significant air-filled karst seen in the respective zone of the video log. A small zone of karst is seen below 23 ft (7 m) but is out of the range of the radar record.

GPR line 42 was the most appropriate radar line in juxtaposition with boreholes PB-28, 25, 8, and 9 (from south to north respectively). The video logs from these boreholes overlain on line 42 can be seen in Figure 5. There is a rather prominent medium amplitude radar reflection that trends across the profile, likely representing a bedding plane (boundary between rock layers) at a

depth of approximately 3 ft (1 m) with associated karst alteration. The borehole logs support this interpretation with a close match of this horizon with air-filled karst in PB-28 and a small cave encountered in PB-25. Deeper zones of karst were seen at a depth of about 20 ft (6 m) in PB-28 and about 36 ft (11 m) in PB-25, the latter just above the position of the water table. No significant karst zone was seen in the PB-8 borehole in association with the radar horizon. A small zone of karst was noted at depth of 5 ft (1.5 m) in PB-9, with no associated radar anomaly. However, it does fall on the trend of the bedding plane horizon.

### **3.2 Supersting resistivity line borehole evaluation**

Eight percussion boreholes associated with resistivity anomalies (encountered during Phase I of this project) on the east and west flanks of the north leg of the excavation and one borehole associated with an anomaly on the south flank of the hilltop excavation were assessed with borehole video. Where possible, the borehole was sited on the resistivity line itself as near to the center location of the resistivity anomaly as possible. In most cases however, the boreholes had to be offset some distance from the resistivity line due to restrictions on working outside the permit area. This issue, together with the positional uncertainty of geologic features giving rise to resistivity anomalies on 2-D profiles (discussed in the first report (SWCA, 2010) as the adjacency effect), necessarily complicates the interpretation of associating karst zones in the video logs to anomalies observed in the resistivity profiles.

One significant resistivity anomaly was observed on ERI Supersting line SS-11 at a depth of approximately 32 ft from the surface. Borehole PB-3 was sited precisely on the ERI line close to the center of the anomaly. Figure 6 shows the location of the borehole and the overlain video log. Three air-filled karst zones (one thick at ~ 14 ft and two thin at ~ 1 - 2 ft) were seen in the borehole at a depth that is consistent with the location and depth of the resistivity anomaly. As described earlier in this report, these zones (unless otherwise described as open caves) consist of highly solution-altered and collapse-altered limestone with a significant fraction (> 20%) of air-filled void space. It is this air space fraction that is likely giving rise to the observed resistivity anomalies.

One significant anomaly observed on ERI line SS-15b at position 94 was assessed with borehole PB-11. This borehole location was offset 10 – 15 ft to the east of the ERI line. A thick zone of air-filled karst at a depth of 48 feet (~ 15 m) in PB-11 coincides well with the position of the resistivity anomaly on the ERI line (Figure 7).

Boreholes PB-12, 13, 17, 19, and 22 were all sited to coincide with the centerpoint of individual ERI anomalies or clusters of anomalies as observed on line SS-02 (Figure 8). However, due to the orientation of the ERI line being slightly outside the project permit area, only PB-12 could be sited directly over the observed anomaly. The rest of the boreholes were offset from

approximately 20 to 40 feet east of the ERI line. Zones of air-filled karst observed in boreholes PB-12 and 13 correspond relatively well to the depth and location of observed ERI anomalies on line SS-02. Zones of karst observed in PB-17, 19, and 22 correspond less well to the observed anomalies, most likely due to lateral changes in karst development in the span of distance between borehole and resistivity line.

The final two boreholes sited outside the excavation footprint coincided with a large and deep resistivity anomaly observed on ERI line SS-08 between positions 45 and 80. These boreholes, PB-16 and PB-20, were drilled less than 10 feet offset to the west of the ERI line (Figure 9). It is apparent from the video log overlay that the depth of the PB-20 borehole was insufficient to reach the observed anomaly. PB-16 does appear to have reached the shallower section of the anomaly albeit with an inconclusive match of a thin observed karst zone with the observed anomaly. This anomaly represents one of the strongest and largest observed on the ERI lines. Its inclination, morphology, and amplitude suggest that this could be a significant well-defined cave as opposed to a zone of air-filled honeycomb/collapse karst. It is entirely possible that borehole PB-16 simply missed it.

### **3.3 Excavation ERI and GPR line borehole evaluation**

Twelve percussion boreholes were drilled and video monitored within the excavation footprint but outside the stilling basin. These boreholes were sited to coincide with near surface (< 25 ft or 8 m) anomalies observed on the ERI Ohm-mapper lines and on the GPR lines acquired within the footprint. Most of the boreholes were completed to a depth of 82 ft (25 m) which was well below the effective depth of the two geophysical techniques used. However, several significant karst zones or actual caves observed in the video logs correlated very well with observed anomalies.

Boreholes PB-1, 2, and 4 were drilled along the central axis of the right arm excavation to confirm observed resistivity and radar anomalies. One ERI Ohm-mapper line (OM-2) was acquired along the central axis of the excavation except in the immediate vicinity of the surface collapse structure where it had to be shifted to the south edge of the excavation to avoid ponded water. Two high resistivity anomalies consistent with caves or air-filled karst were observed on either side of the collapse structure. The video log of borehole PB-1 shows a distinct zone of air-filled karst at a depth of 20 ft. that is consistent with the location and depth of the anomaly on the west side (Figure 10). In addition, a network of air-filled solution-enlarged fractures observed on the floor of the excavation in the immediate vicinity of the location of PB-1 and 2 is consistent with the zone of karst observed in the first meter of the PB-1 borehole. Borehole PB-2 is not shown on Figure 10 due to its proximity to PB-1. No air-filled karst zones were observed in the first 20 ft (6 m) of borehole PB-4. Likewise, no high resistivity anomalies were observed in the OM-2 ERI line at the location of the borehole. Beginning at 45 ft in PB-4 a very significant zone

of air-filled karst (approximately 20 ft thick) was observed in the video log. Given a top hole elevation of 765 ft for PB-4, the top of this karst zone at ~ 720 ft is consistent with the karst honeycomb observed at the base of the creekside bluff upstream from the excavation.

Given the shallow penetration of the GPR lines (< 10 ft) along this section of the excavation (co-located with the OM-2 line) no attempt was made to correlate the PB-1, 2, and 4 video logs with the GPR results.

Nine boreholes were completed within the footprint of the left arm excavation, 3 along the central axis of the excavation coincident with the OM-3 resistivity line, and 3 each coincident with the OM-5 and OM-4 resistivity lines that were offset approximately 10 ft (3 m) to the east and west of the central axis. Figure 11 shows the OM-3 line with overlays of the PB-14, 27, and 18 video logs. There is a clear correlation of a moderately thick (7 – 9 ft) air-filled karst zone in the PB-14 and 18 video logs with a strongly resistive anomaly in the OM-3 line. PB-27, a shallow hole drilled approximately 30 ft north of PB-14, encountered a karst zone at the 25 ft depth level. This zone may correlate with a slightly deeper resistive anomaly adjacent to the borehole and just visible at the bottom of the OM-3 profile.

Three boreholes, PB-15, 26, and 29 were completed along the OM-4 resistivity line (Figure 12). PB-29 was drilled immediately adjacent to PB-26 and as it served as a secondary hole for the cave encountered in PB-26 it did not provide any new information. PB-29 will not be discussed further. In borehole PB-15, one thin air-filled karst zone was encountered at approximately 13 ft below the surface. There is no strong resistive anomaly observed on line OM-4 in association with this zone. However, there is a medium resistive feature adjacent to the borehole at a similar depth level to this karst zone. This feature has a subtle dip angle and may be associated with bedding plane karst. The most significant feature encountered in any borehole was a substantial cave encountered between depth levels 18 – 21.5 ft in borehole PB-26. The cave appeared to be laterally extensive (> 20 ft) from evaluation of the video. Unfortunately, the borehole location was at the very end of the resistivity line OM-4 and the cave was not detected, most likely due to poor data coverage common to the ends of resistivity profiles. The cave (or cave roof) is clearly visible in the collocated GPR line also shown in Figure 12. Proper evaluation of this cave's lateral extent and depth can only be accomplished by drilling a sufficiently large borehole to permit entry by qualified cavers familiar with cave surveying and exploration.

Three boreholes, PB-21, 23, and 24 were completed along the OM-5 resistivity line (Figure 13), all situated toward the north end of the excavation. The overlay of the PB-21 video log and the relative absence of air-filled karst zones suggest that the borehole may have just missed the large resistive anomaly that was the intended target. Further down the PB-21 borehole at a depth of 53 ft., a 14 ft. thick zone of air-filled karst was observed. However, this was well below the depth range of the OM-5 resistivity line. Borehole PB-23 encountered two significant zones of air-

filled karst and one small cave or large void (~ 1ft) at a depth of 45 ft.. The upper zone of karst correlated well with a resistive anomaly observed on the OM-5 line; the void and lower zone of karst fell below the depth range of the OM-5 line. The final borehole, PB-24, was completed at the far end of the OM-5 line, where insufficient data exists to make a correlation to the video log. Of interest though is a small cave 22 feet below the surface with a ceiling to floor height of 3 ft. This cave was encountered at a similar level to the large cave encountered in PB-26. Below the cave is a substantial thickness (in multiple zones) of air-filled karst.

#### **4.0 CONCLUSIONS**

Twenty-eight percussion boreholes were drilled and 26 were video-logged within the project area of the Dry Comal Creek Flood Retarding Structure for the purposes of correlating observed karst development within the boreholes to resistivity and radar anomalies observed on multiple geophysical transects collected during Phase I (SWCA, 2010) of this investigation. With the limited borehole information available during Phase I, near-surface radar anomalies (as higher amplitude reflections in contrast with the background returns) were interpreted as actual voids (small caves) and/or air-filled karst developed along solution-altered bedding planes, fractures, or collapse zones. Resistivity anomalies observed from the ERI program in Phase I were interpreted as small to large air-filled caves. This new set of important data from the borehole program has modified our interpretation to some degree. With regard to GPR, there was sufficient correlation of anomalous high-amplitude radar reflections in the stilling basin GPR profiles with observed zones of air-filled karst in the boreholes to conclude a causal relationship. In addition, the position and depth of the cave encountered in PB-26 matched quite well with the strong radar reflections observed in the respective GPR profile. Our summary conclusion with respect to the GPR data is that there is a high probability that the higher amplitude radar reflections seen in the stilling basin and excavation profiles represent localized karst development with varying degrees of air-filled void space, quite possibly in the 10 – 30% range of total rock volume. The majority of the karst is likely related to honeycomb solution and collapse of rock units within the Leached and Collapsed Member of the Edwards limestone.

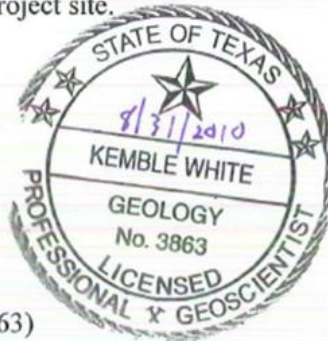
With regard to ERI, there is sufficient correlation of air-filled collapse and honeycomb karst zones observed in the boreholes with the high resistivity anomalies observed in both the Supersting and Ohm-mapper ERI profiles to conclude that this type of karst (often referred to in the literature as mesocavern karst) is capable of generating as equally high resistivity values as that generated by large open void spaces such as caves. This new interpretation, however, does not preclude the existence of cavernous space within the project area and underlying the excavation footprint. Some of the stronger resistivity anomalies may include both mesocavern and cave development – the latter simply missed by the single boreholes drilled for each anomaly.

In summary, both the GPR and ERI anomaly results have been largely confirmed by observed mesocavern karst and cave development in the percussion boreholes.

References

SWCA Environmental Consultants, 2010. Geophysical Survey and Assessment of Karst Geology, Dry Comal Creek Flood Retarding Structure, Comal County, Texas. A report prepared for Freese and Nichols, Inc. February 24, 2010.

As a licensed professional geoscientist I attest that the geological interpretations contained within this report were developed by me and Dr. Blake Weissling in conjunction with other project P.G.s. They are consistent with available published geologic maps and with site specific geologic work conducted by me and under my supervision on the project site.



Kemble White, Ph.D., P.G. (TX3863)

West

PB-5

East

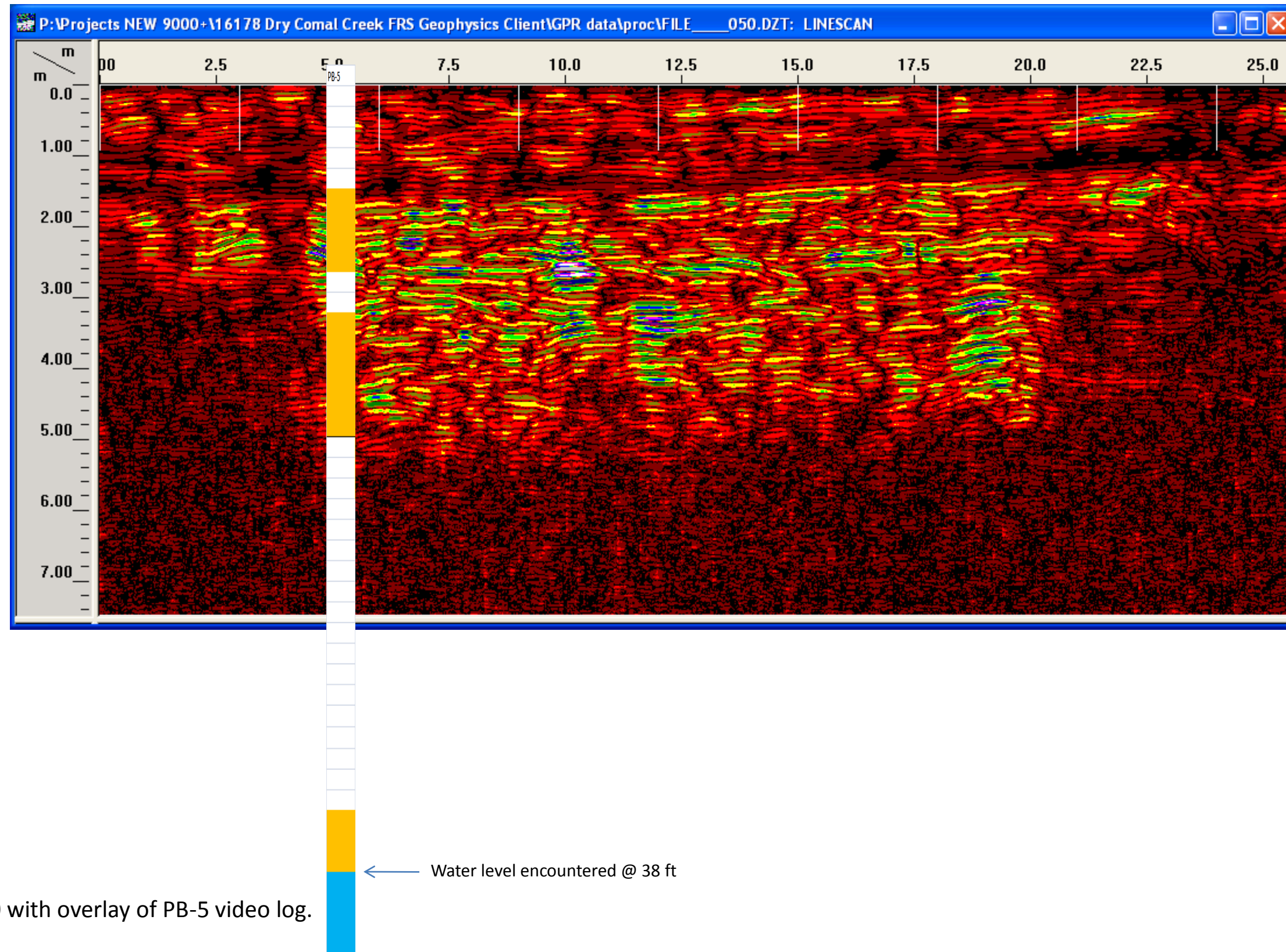


Figure 1. GPR line 50 with overlay of PB-5 video log.

South  
PB-6

North

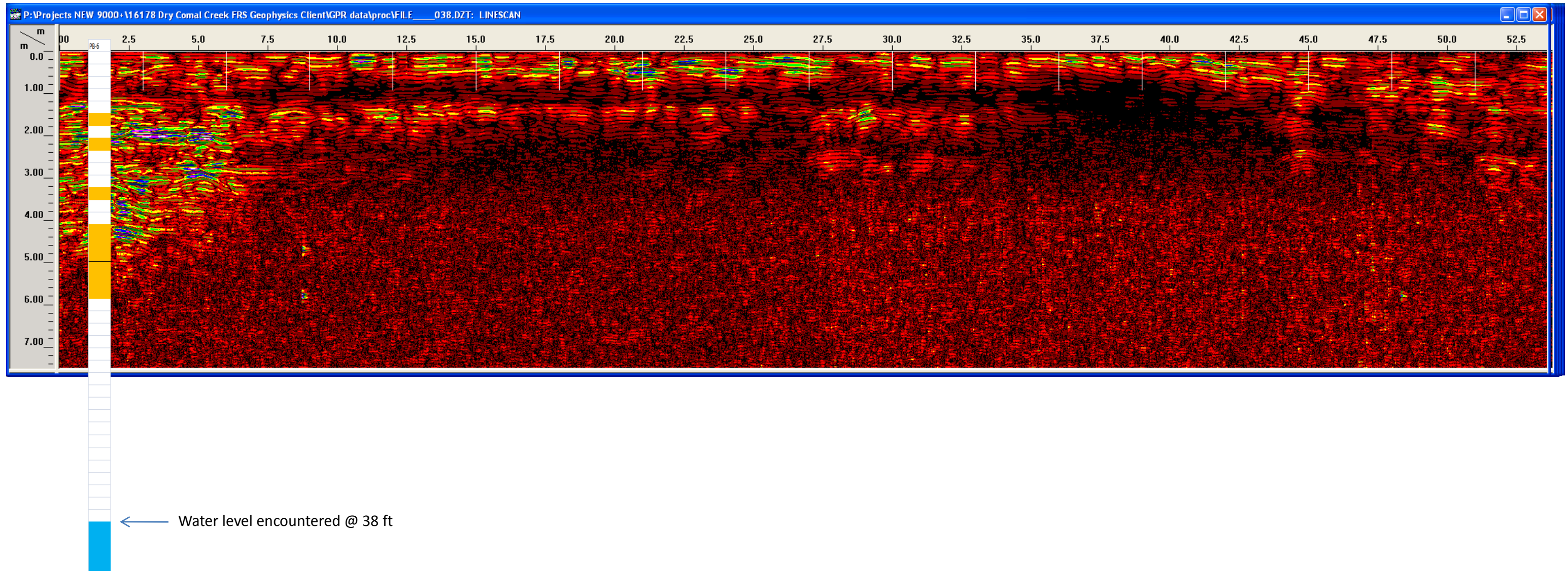


Figure 2. GPR line 38 with overlay of PB-6 video log.

South

North

PB-7

PB-10

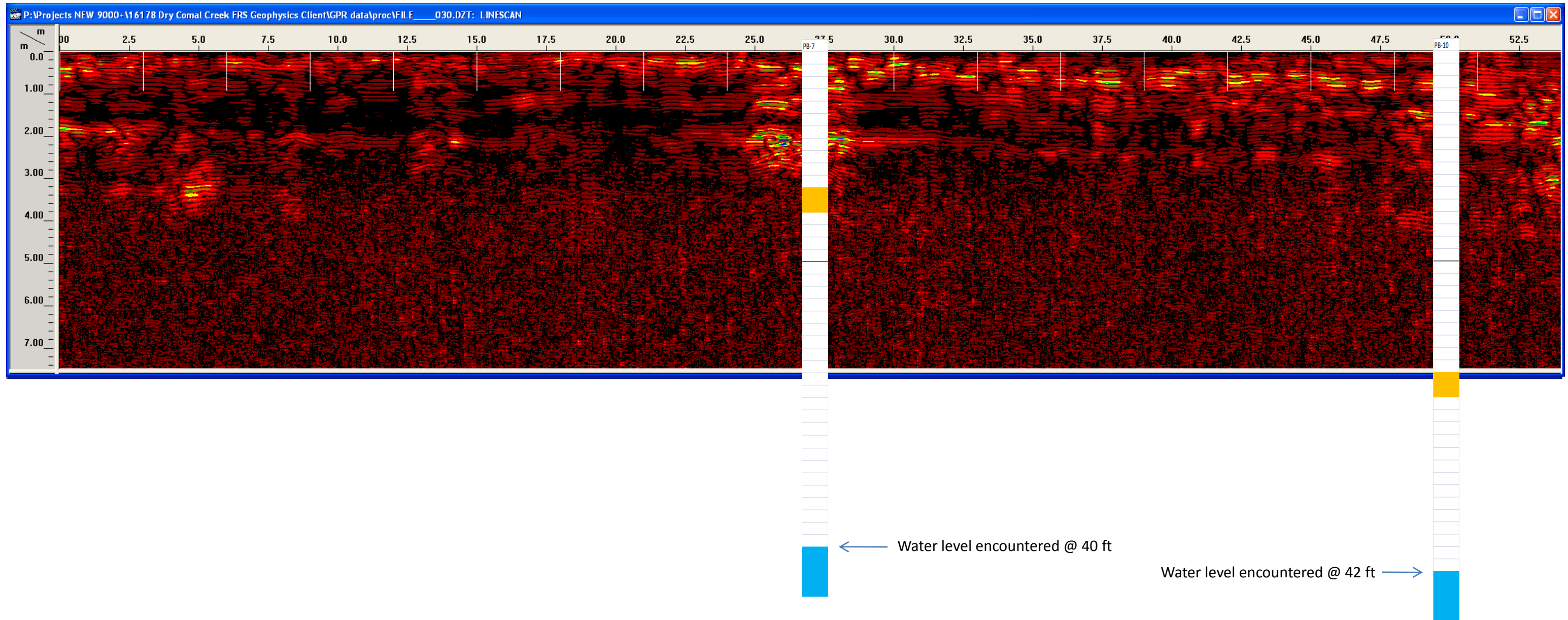


Figure 3. GPR line 30 with overlay of PB-7 and PB-10 video logs.

North

South

PB-10

PB-7

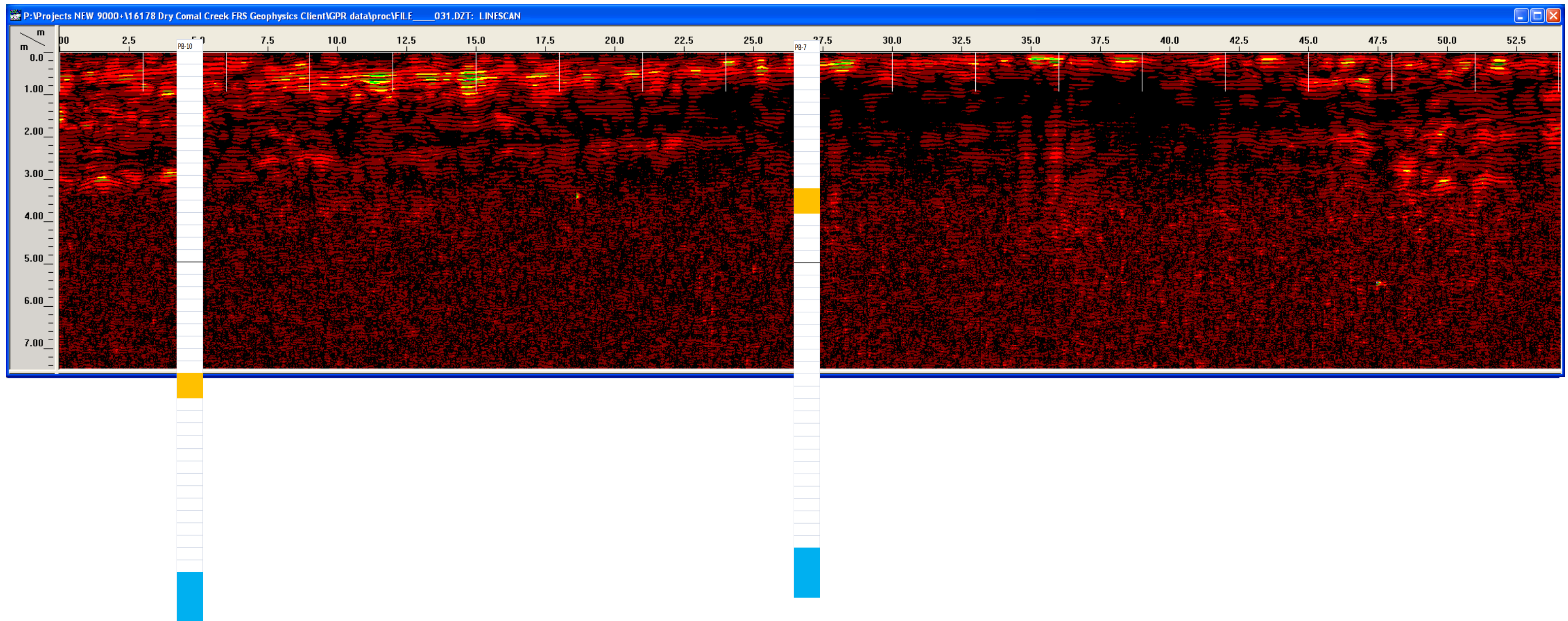


Figure 4. GPR line 31 with overlay of PB-7 and PB-10 video logs.

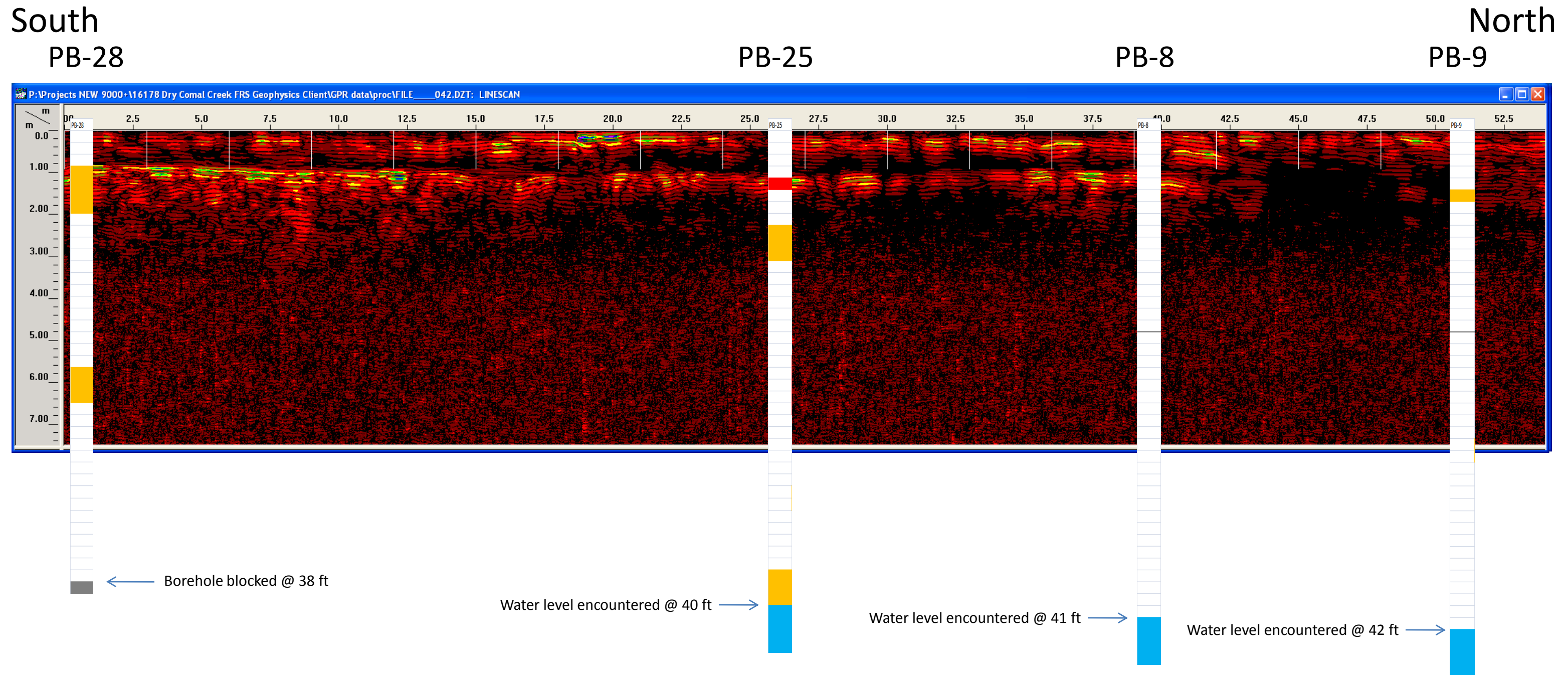


Figure 5. GPR line 42 with overlay of PB-28, PB-25, PB-8, and PB-9 video logs.

# Line SS-11

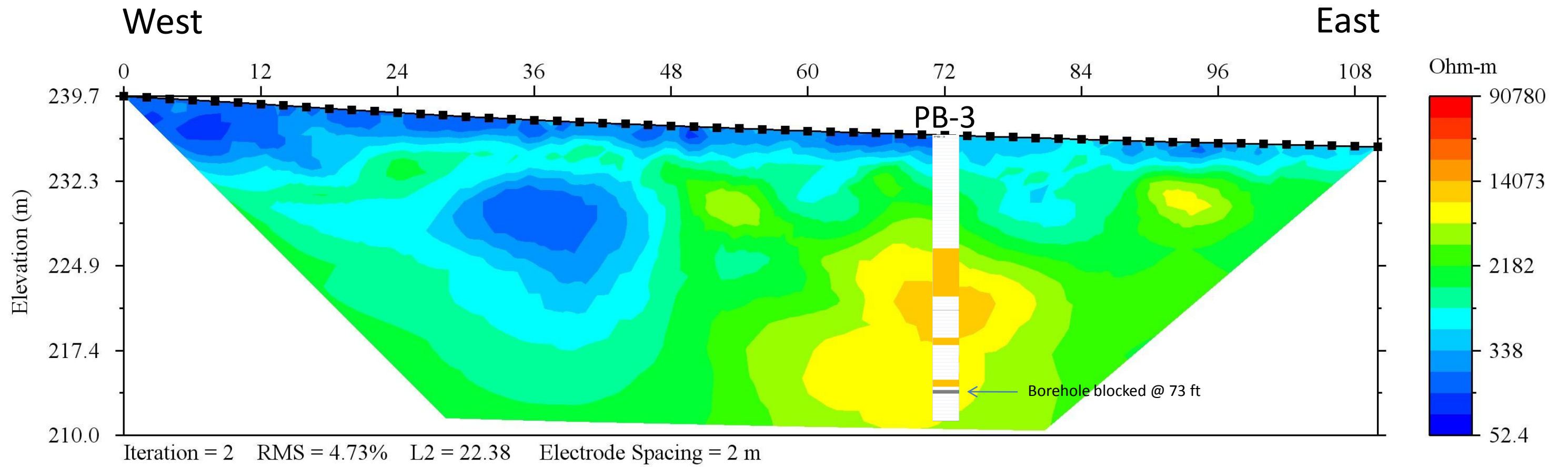


Figure 6. ERI line SS-11 with overlay of PB-3 video log.C

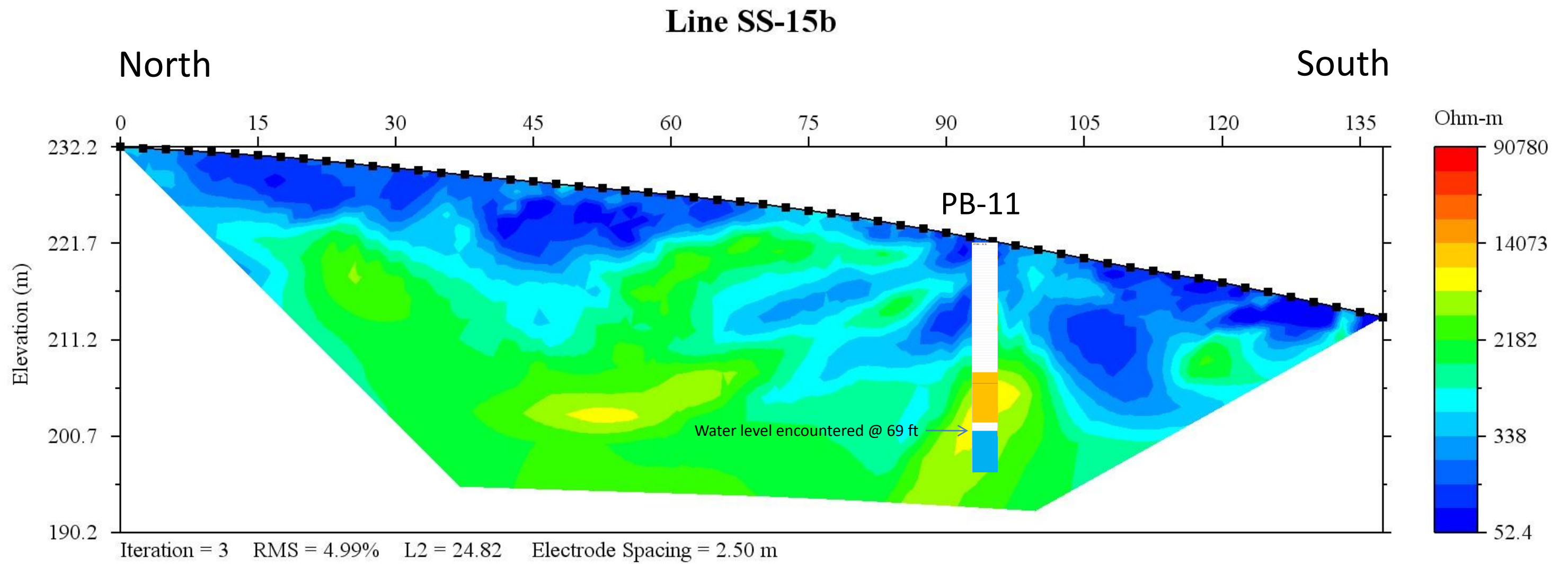


Figure 7. ERI line SS-15b with overlay of PB-11 video log.

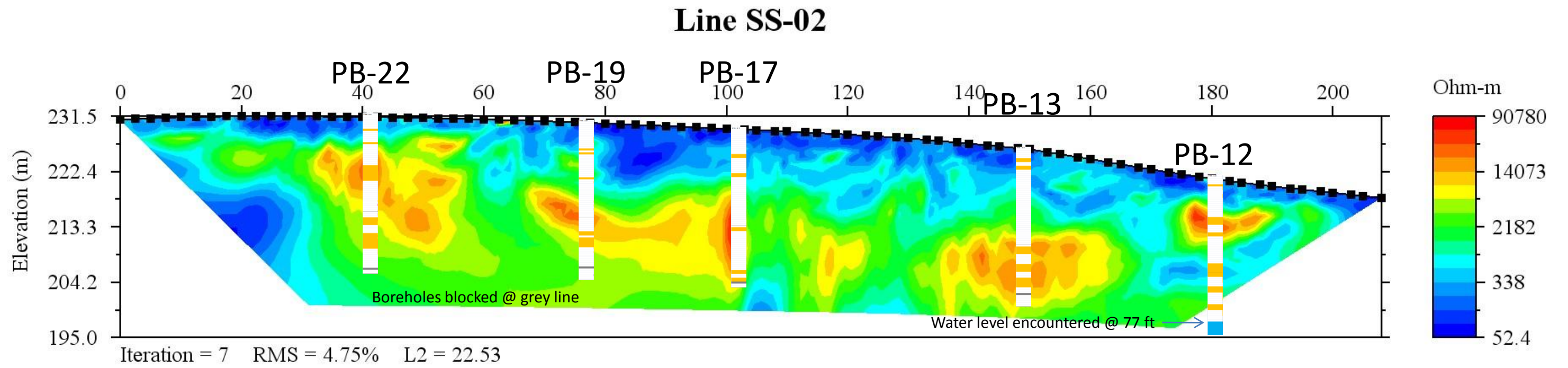


Figure 8. ERI line SS-02 with overlay of PB-22, PB-19, PB-17, PB-13, and PB-12 video logs.

# Line SS-08

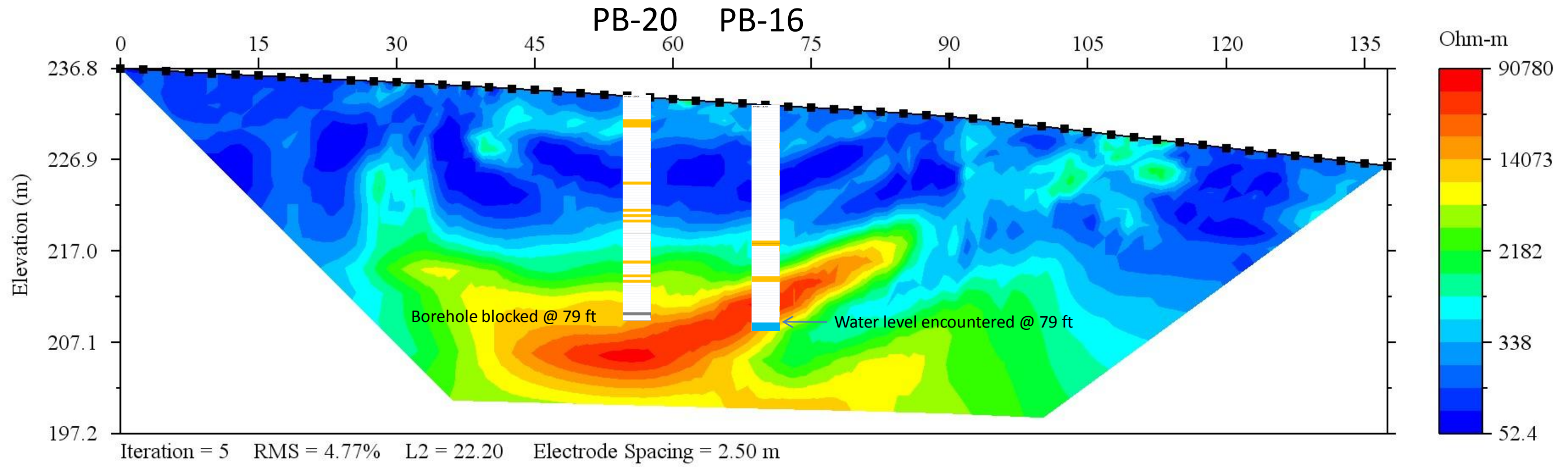


Figure 9. ERI line SS-08 with overlay of PB-20 and PB-16 video logs.

# Line OM-02

West

East

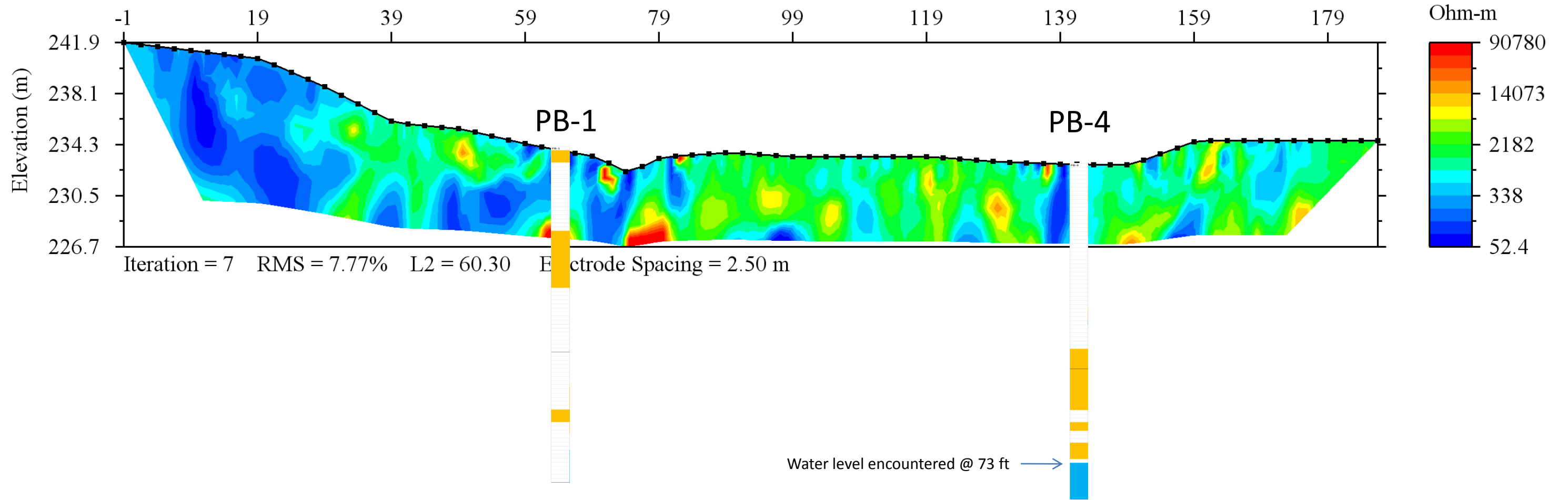


Figure 10. Ohm-Mapper line OM-2 with overlays of PB-1 and PB-4 video logs.

# Line OM-03

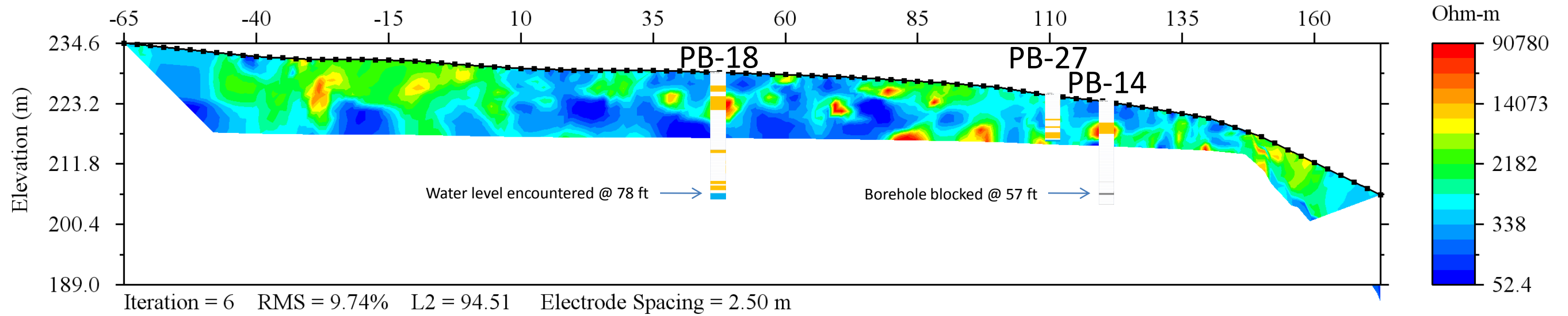


Figure 11. Ohm-Mapper line OM-3 with overlays of PB-18, PB-27, and PB-14 video logs.

# Line OM-04

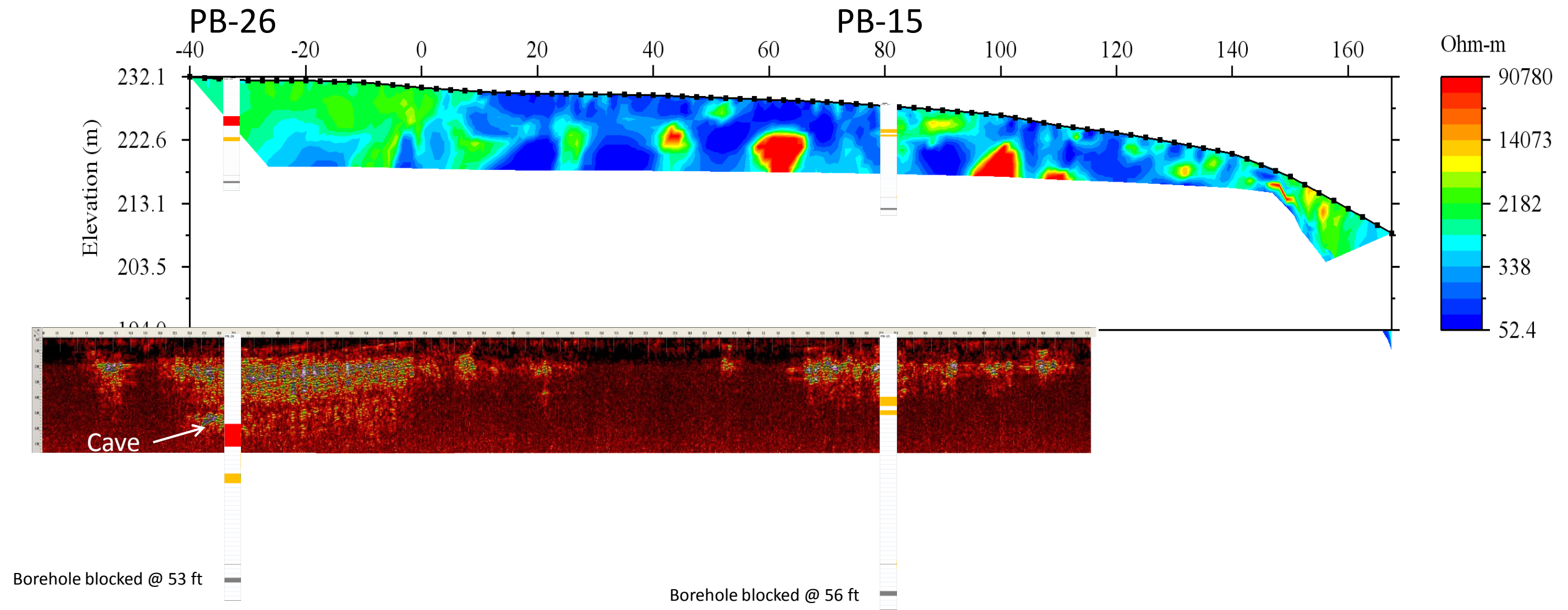


Figure 12. Ohm-Mapper line OM-4 and colocated GPR line with overlays of PB-26 and PB-15 video logs.

# Line OM-05

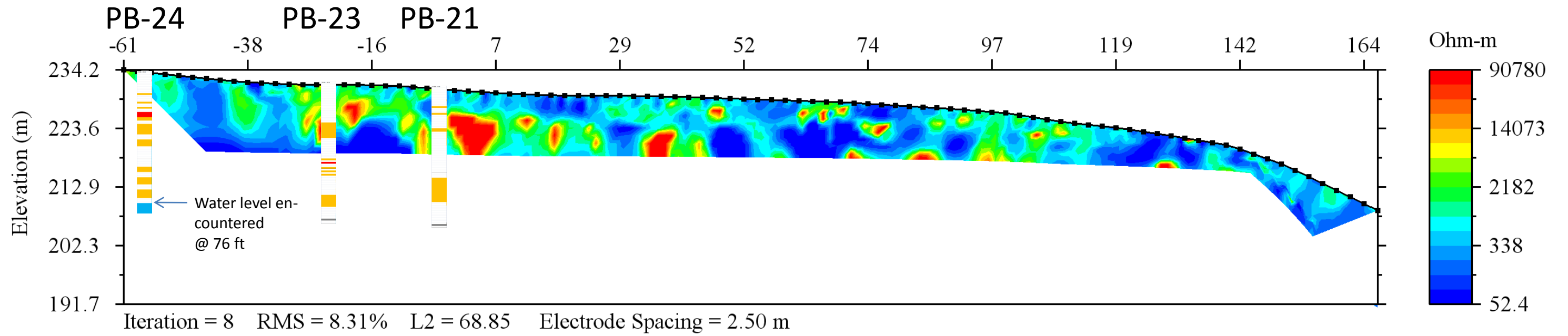


Figure 13. Ohm-Mapper line OM-5 with overlays of PB-24, PB-23, and PB-21 video logs.